What controls the seasonal cycle of columnar methane observed by GOSAT over different regions in India.

Naveen Chandra[1*], Sachiko Hayashida[1], Tazu Saeki[2], and Prabir K. Patra[2]

[1] Nara Women's University, Kita-Uoya Nishimachi, Nara 630-8506, Japan

[2] Department of Environmental Geochemical Cycle Research, JAMSTEC, Yokohama 2360001, Japan

Correspondence to: Naveen Chandra (nav.phy09@gmail.com)

Abstract. Methane (CH_4) is one of the most important short-lived climate forcers for its critical roles in greenhouse warming and air pollution chemistry in the troposphere, and water vapor budget in the stratosphere. It is estimated that up to about 8% of global CH_4 emissions occur from South Asia, covering less than 1% of the global land. With the availability of satellite observations from space, variability in CH_4 have been captured for most parts of the global land with major emissions, which were otherwise not covered by the surface observation network. The satellite observation of the columnar dry-air mole fractions of methane (XCH_4) is an integrated measure of CH_4 densities at all altitudes from the surface to the top of the atmosphere. Here, we present an analysis of XCH_4 variability over different parts of India and the surrounding cleaner oceanic regions as measured by Greenhouse gases Observation SATellite (GOSAT) and simulated by an atmospheric chemistry-transport model (ACTM). Distinct seasonal variations of XCH_4 have been observed over the northern (north of 15^{o}N) and the southern part (south of 15^{o}N) of India, corresponding to the peak during southwest monsoon (July-September) and early autumn season (October-December), respectively. Analysis of the transport, emission and chemistry contributions to XCH_4 using ACTM suggests that distinct XCH_4 seasonal cycle over northern and southern regions of India is governed by the both heterogeneous distributions of surface emissions and contribution of the partial CH_4 column in the upper troposphere. Over most part of the northern Indian Gangetic Plain regions, up to 40% of the peak-to-trough amplitude during the southwest (SW) monsoon season is attributed to the lower troposphere (~1000-600 hPa), while ~40% to uplifted high-CH_4 air masses in the upper troposphere (~600-200 hPa). In contrast, the XCH_4 seasonal enhancement over the semi-arid western India is attributed mainly (~70%) to the upper troposphere. The lower tropospheric region contributes up to 60% in the XCH_4 seasonal enhancement over the southern peninsula and oceanic region. These differences arise due to the complex atmospheric transport mechanisms, caused by the seasonally varying monsoon. The CH_4 enriched air mass is uplifted from high emission region of the Gangetic Plain by the SW monsoon circulation and deep cumulus convection and then confined by anticyclonic wind in the upper tropospheric heights (~200 hPa). The anticyclonic confinement of surface emission over a wider South Asia region leads to strong contribution of the upper troposphere in the formation of the XCH_4 peak over northern India, including the semi-arid regions with extremely low CH_4 emissions. Based on this analysis, we suggest that a link between surface emissions and higher levels of XCH_4 is not always valid over Asian monsoon regions, although there is often a fair correlation between surface emissions and XCH_4. The overall validity of ACTM simulation for capturing GOSAT observed seasonal and spatial XCH_4 variability will allow us to perform inverse modelling of XCH_4 emissions in the future using XCH_4 data.

1. Introduction

Methane (CH_4) is the second most important anthropogenic greenhouse gas (GHG) after carbon dioxide (CO_2) and accounts for ~20% (+0.97 W m^{-2}) of the increase in total direct radiative forcing, since 1750 (Myhre et al., 2013). CH_4 is emitted from a range of anthropogenic and natural sources on the Earth's surface into the atmosphere. The main natural sources of CH_4 include wetlands and termites (Matthews and Fung, 1987; Cao et al., 1998; Sugimoto et al., 1998). Livestock, rice cultivation, fossil fuel industry (production and uses of natural gas, oil, and coal) and landfills are the major sectors among the anthropogenic sources (Crutzen et al., 1986; Minami and Neue; 1994, Olivier et al., 2006; Yan et al., 2009). These results also suggest that the Asian region is emission hotspot of CH_4 due to the large number of livestock, intense cultivation, coal mining, waste management and other anthropogenic activities (EDGAR2FT, 2013).

With a short atmospheric lifetime of about 10 years (e.g., Patra et al., 2011a) and having 34 times more potential to trap heat than CO_2 on mass basis over a 100-year timescale (Gillett and Matthews, 2010, Myhre et al., 2013), mitigation of CH_4 emissions could be the most important way to limit global warming at inter-decadal time scales (Shindell et al., 2009). Better knowledge of CH_4 distribution and quantification of its emission flux is indispensable for assessing possible mitigation strategies. However, sources of CH_4 are not yet well quantified due to sparse ground based measurements, which results in limited representation of CH_4 flux on a larger scale (Dlugokencky et al., 2011; Patra et al., 2016). Recent technological advances have made it possible to detect spatial and temporal variations in atmospheric CH_4 from space (Frankenberg et al., 2008; Kuze et al., 2009), which could fill the gaps left by ground, aircraft and ship-based measurements, albeit at a lower accuracy than the *in situ* measurements. Further, despite the satellite observations having an advantage of providing continuous monitoring over a wide spatial range, the information obtained from passive nadir-sensors that use solar radiation at Short-Wavelength Infrared (SWIR) spectral band, is limited to columnar dry-air mole fractions of methane (XCH_4). This is an integrated measure of CH_4 with contributions from the different vertical atmospheric layers, i.e., from the measurement point on the Earth's surface to the top of the atmosphere (up to about 100km or more precisely to the satellite orbit).

The South Asia region, consisting of India, Pakistan, Bangladesh, Nepal, Bhutan and Sri Lanka, exerts a significant impact on the global CH_4 emissions, with regional total emissions of 37±3.7 Tg-CH_4 of about 500 Tg-CH_4 global total emissions during the 2000s (Patra et al., 2013). The Indo-Gangetic Plain (IGP) located in the foothills of the Himalayas is one of the most polluted regions in the world, which hosts 70% of coal-fired thermal power plants in India and experiences intense agricultural activity (Kar et al., 2010). This region is of particular interest mainly due to the coexistence of deep convection and large emission of pollutants (including CH_4) from a variety of natural and anthropogenic sources. Rainfall during the SW monsoon season cause higher CH_4 emissions from the paddy fields and wetlands (e.g., Matthews and Fung, 1987; Yan et al., 2009; Hayashida et al., 2013) while the persistent deep convection results the updraft of CH_4-laden air mass from the surface to the upper troposphere during the same season, which is then confined by anticyclonic winds at the this height (Patra et al., 2011b; Baker et al., 2012; Schuck et al., 2012). Several other studies also have highlighted the role of convective transport of pollutants (including CH_4) from surface to the upper troposphere (400 – 200 hPa) during SW monsoon season (July-September) (Park et al., 2004; Randel et al., 2006; Xiong et al., 2009; Lal et al., 2014, Chandra et al., 2016). The dynamical system dominated by deep convection and anticyclone cover mostly the northern Indian region (north of 15^{o}N) due to the presence of the Himalayas and the Tibetan Plateau, while such complex dynamical system has not been observed over the southern part of India (south of 15^{o}N) (Rao, 1976).

Satellite-based measurements show elevated levels of XCH_4 over the northern part of India (north of 15°N) particularly high over IGP during the SW monsoon season (July to September) and over southern India (south of 15°N) during early autumn season (October to December) (Frankenberg et al., 2008, 2011; Hayashida et al., 2013). Previous studies have linked these high XCH_4 levels to the strong surface CH_4 emissions particularly from the rice cultivation over the Indian region because they showed statistically significant correlations over certain regions (Hayashida et al., 2013; Kavitha et al., 2016). The differences in the peak of XCH_4 seasonal cycle over northern and southern regions of India are also discussed on the basis of agricultural practice in India that takes place in two seasons, May to October and November to April, respectively. However, inferring local emissions directly from variations in XCH_4 is ambiguous particularly over the Indian regions under the influence of monsoon meteorology, because XCH_4 involves contributions of CH_4 abundances from all altitudes along the solar light path.

This study attempts for the first time to separate the factors responsible (emission, transport, and chemistry) for the distributions of columnar methane (XCH_4) over the Asian monsoon region for different altitude segments. The XCH_4 mixing ratios are used for this study as observed from GOSAT and simulated by JAMSTEC's ACTM. We aim to understand relative contributions of surface emissions and transport in the formation of XCH_4 seasonal cycles over different parts of India and the surrounding oceans. This understanding will help us in developing an inverse modelling system for estimation of CH_4 surface emissions using XCH_4 observations and ACTM forward simulation.

2. Methods

2.1 Satellite data:

The Greenhouse gases Observing SATellite (GOSAT) (also referred to as Ibuki) project is developed jointly by the National Institute for Environmental Studies (NIES), Ministry of the Environment (MOE) and Japan Aerospace Exploration Agency (JAXA). It has been providing columnar dry air mole fractions of the two important greenhouse gases (XCH_4 and XCO_2) at near global coverage since its launch in January 2009. It is equipped onboard with the Thermal And Near infrared Sensor for carbon Observation-Fourier Transform Spectrometer (TANSO-FTS) and the Cloud and Aerosol Imager (TANSO-CAI) (Kuze et al., 2009). To avoid cloud contamination in the retrieval process, any scene with more than one cloudy pixel within the TANSO-FTS IFOV is excluded. The atmospheric images from CAI are used to identify the cloudy pixels. As a result of this strict screening, only limited numbers of XCH_4 data are available during the SW monsoon over South Asia. This study uses the GOSAT SWIR XCH_4 (Version 2.21)-Research Announcement product for the period of 2011-2014. The ground-based FTS measurements of XCH_4 by the Total Carbon Column Observing Network (TCCON) (Wunch et al., 2011) are used extensively to validate the GOSAT retrievals. Retrieval bias and precision of column abundance from GOSAT SWIR observations have been estimated as approximately 15-20 ppb and 1%, respectively for the NIES product using TCCON data (Morino et al., 2011; Yoshida et al., 2013).

2.2. Model simulations

Model analysis is comprised of simulations from the JAMSTEC's atmospheric general circulation model (AGCM)-based chemistry-transport model (ACTM; Patra et al., 2009). The AGCM was developed by the Center for Climate System Research/National Institute for Environmental Studies/Frontier Research Center for Global Change (CCSR/NIES/FRCGC). It has been parts of the transport model intercomparison experiment TransCom-CH_4 (Patra et al., 2011a) and used in inverse

modeling of CH_4 emissions from in situ observations (Patra et al., 2016). The ACTM runs at a horizontal resolution of T42 spectral truncations (~$2.8^O \times 2.8^O$) with 67 sigma-pressure vertical levels. The evolution of CH_4 at different longitude (x), latitude (y) and altitude (z) with time in the Earth's atmosphere depends on the surface emission, chemical loss, and transport, which can be mathematically represented by the following continuity equation:

$$\frac{dCH_4(x,y,z,t)}{dt} = S_{CH4}(x,y,t) - L_{CH4}(x,y,z,t) - \nabla.\phi(x,y,z,t)$$

where

CH_4 = methane burden in the atmosphere

S_{CH4} = Total emissions/sinks of CH_4 at the surface

L_{CH4} = Total loss of CH_4 in the atmosphere due to the chemical reactions

$\nabla.\phi$ = Transport of CH_4 due to the advection, convection and diffusion.

The meteorological fields of ACTM are nudged with reanalysis data from the Japan Meteorological Agency, version JRA-25 (Onogi et al., 2007). The model uses an optimal OH field (Patra et al., 2014) based on a scaled version of the seasonally varying OH field (Spivakovsky et al., 2000). The a priori anthropogenic emissions are from Emission Database for Global Atmospheric Research (EDGAR) v4.2 FT2010 database (http://edgar.jrc.ec.europa.eu). The model sensitivity for emission is examined by two cases of emission scenarios based on different combination of sectoral emissions. First one is referred to the 'AGS', where all emission sectors in EDGAR42FT are kept at a constant value for 2000, except for emissions from agriculture soils. The second one is controlled emission scenario referred to 'CTL', which is based on the ensemble of the anthropogenic emissions from EDGAR32FT (as in Patra et al., 2011a), wetland and biomass burning emissions from Fung et al. (1991) and rice paddies emission from Yan et al. (2009). The emission seasonality differs substantially between the CTL case and the AGS case due to differences in emissions from wetlands, rice paddies, and biomass burning; other anthropogenic emissions do not contain seasonal variations (Patra et al., 2016). Further details about the model and these emission scenarios can be found in the previous studies (Patra et al., 2009; Patra et al., 2011a; Patra et al., 2016).

XCH_4 is calculated from the ACTM profile using following equations:

$XCH_4 = \Sigma_{n=1}^{60} CH_4(n) \times \Delta\sigma_p(n)$

where, CH_4 (n) is the dry-air mole fraction at model mid-point level, n = number of vertical sigma pressure layers of ACTM (= 1-60 with σ_p values of 1.0 and 0.005), $\Delta\sigma_p$ = thickness of Sigma pressure level. Note here that we have not incorporated convolution of model profiles with retrieval a priori and averaging kernels. Because the averaging kernels are nearly constant in the troposphere (Yoshida et al., 2011), hence this approximation does not lead to serious errors in constructing the model XCH_4. For both the CTL and AGS cases, we adjust a constant offset of 20 ppb to the modeled time series, which should make the *a priori* correction have a lesser impact on the model XCH_4. Because the focus of this study is seasonal and spatial variations in XCH_4, a constant offset adjustment should not affect the main conclusions.

3. Results and discussion

3.1 XCH_4 over the Indian region: View from GOSAT and ACTM simulations

This section presents an analysis of XCH_4 observed by GOSAT from Jan 2011 to Dec 2014 over the Indian region. We characterize the 4 seasons specific to the region as winter (January to March), spring (April to June), summer (July to September) or the SW monsoon, and autumn (October to December) as commonly used in meteorological studies (e.g., Rao, 1976). To study the seasonal XCH_4 pattern in details depending on the distinct spatial pattern of surface emissions and XCH_4 mixing ratios shown in Figure 1, the Indian landmass was partitioned into eight sub-regions: Northeast India (NEI), Eastern India (EI), Eastern IGP (EIGP), Western IGP (WIGP), Central India (CI), Arid India (AI), Western India (WI), Southern Peninsula (SP), and two surrounding oceanic regions, the Arabian Sea (AS) and Bay of Bengal (BOB) (Figure 2a). Regional divisions are made based on spatial patterns of emission and XCH_4 (Figure 1a1-c2), and our knowledge of seasonal meteorological conditions. Since general features of XCH_4 simulated by ACTM using emission scenarios AGS and CTL are similar to each other, the main discussion is made using AGS scenario only.

Figure 1a1-a2 show that the XCH_4 mixing ratios are lower in spring and higher in autumn. A strong latitudinal gradient in XCH_4 is observed between the Indo-Gangetic Plain (IGP) and the other parts of India. XCH_4 show the highest value (~1880 ppb) over the IGP, eastern and northeast Indian regions. As seen from Figure 1b1-b2, ACTM simulations are able to reproduce the observed latitudinal and seasonal gradients in XCH_4; i.e., higher values during the southwest monsoon and autumn seasons and lower values during the winter and spring seasons over the IGP region. The optimized total CH_4 fluxes (AGS and CTL) show high emissions over the IGP region and northeast Indian regions (Figure 1c1-c2). Most elevated levels of XCH_4 are often observed simultaneously with the higher emissions, suggesting a link between the enhanced XCH_4 and high surface emissions in summer. However, this link is not valid for all locations. For example, over the western and southern region of India, XCH_4 is higher in autumn than in spring, though the emissions are higher in spring.

Figure 2b-k shows ACTM - GOSAT comparisons of XCH_4 time series from Jan 2011 to Dec 2014 over the selected study regions. The simulated XCH_4 data are sampled at the nearest model grid to the available GOSAT observations and at the satellite overpass time (~ 1300 LT) and then averaged over each study region. Observations are sparse or not available during the SW monsoon season in some of the regions due to limitations of GOSAT retrieval under cloud cover. The model captures the salient features of the seasonal cycles at very high statistical significance (correlation coefficients, $r > 0.8$; except for NE India; Table 1). The high ACTM-GOSAT correlations for the low/no emission regions suggest that transport and chemistry are accurately modeled in ACTM. Although we do not have the statistically significant number of observations for the SW monsoon period, the observed high GOSAT XCH_4 are generally well simulated by ACTM over most of the study regions. Based on these comparisons, we can assume that model simulations can be used to understand XCH_4 variability over the Indian region. Though we showed only the paired GOSAT and ACTM data that matched in time and location in Figure 2b-k, we also confirmed that the correlation is high (r~0.9) between the monthly-averaged time series of GOSAT and ACTM averaged for the four years (2011-2014) when ACTM is not co-sampled at the GOSAT sampling points (Figure S1). These high correlations assure representativeness of the data shown in Figure 2b-k. Thus, the seasonal evolution of XCH_4 using the ACTM simulations alone is expected to be fairly valid for different altitude layers (ref. to Patra et al., 2011b for comparison at the aircraft cruising altitude). Though the model is only validated for XCH_4 in this study, comparisons with surface and independent aircraft CH_4 observations have been shown in Patra et al. (2016).

3.2 Seasonal cycle of XCH_4 and possible controlling factors

As mentioned earlier, that the persistent deep convection and mean circulation during the SW monsoon season significantly enhance CH_4 in the upper troposphere (e.g., Xiong et al., 2009, Baker et al., 2012), coinciding with the period of high surface CH_4 emissions due to rice paddy cultivation and wetlands over the Indian region (Yan et al., 2009; Hayashida et al., 2013). Although both these emissions and transport processes contribute greatly to seasonal changes in XCH_4, their relative contributions have not been studied over the monsoon dominated Indian region.

For understanding the role of transport, the atmospheric column is segregated into five sigma-pressure (σ_p) layers, starting from the surface level ($\sigma_p = 1$) to top of the atmosphere ($\sigma_p = 0$), with an equal layer thickness of $\sigma_p = 0.2$. Lower Troposphere (LT), Mid-Troposphere1 (MT1), Mid-Troposphere2 (MT2), Upper Troposphere (UT) and Upper Atmosphere (UA) denote the layers corresponding to the sigma pressure values of 1.0-0.8, 0.8-0.6, 0.6-0.4, 0.4-0.2, and 0.2-0.0. The partial columnar CH_4 are calculated within different σ_p layers (denoted by X_pCH_4) using the same formula for XCH_4, as in Section 2.2. The model results are averaged over each sub-region of our analysis for XCH_4 seasonal cycle. For understanding the role of surface emission in the XCH_4 seasonal cycle, the climatology of optimized total CH_4 flux for each sub-region are compared. Figure 3 shows the monthly mean climatology (average for 2011-2014) of total CH_4 flux, XCH_4 and X_pCH_4 from the model averaged over three selected regions, EIGP (a1-a7), SP (b1-b7) and AI (c1-c7). These representative regions have been selected because they show distinct XCH_4 seasonal cycles and the dominant controlling factors (such as emission, transport, and chemistry). The observed GOSAT XCH_4 values are also shown for a reference, because the model results do not correspond to the location and time of GOSAT observations (as opposed to those in Figure 2). The plots for the remaining seven regions are available in the supplementary Figures S2 and S3.

Over the EIGP region, magnitude and timing of the seasonal peak in emission differ substantially between the CTL and AGS emission scenarios (ref. Figure 3a7). ACTM simulated XCH_4 seasonal peak is in agreement with the peak in emission in June for AGS case (Figure 3a6). However, simulated XCH_4 remains nearly constant until September, although the emission decreases substantially toward winter. In general, the emission is relatively higher in monsoon season (July-August-September) than in other seasons in both cases. However, in the LT, where we expect most susceptible to the surface emission, the partial column CH_4 indicates very different seasonality from the emissions; X_pCH_4 (LT) increases toward winter continuously (Figure 3a5). The partial CH_4 columns for the upper troposphere and middle troposphere (Figure 3a2-a3) show similar seasonality to the total XCH_4 rather than in the LT. Therefore, this analysis strongly suggests that the emissions from surface and the upper tropospheric partial column, both contribute to the formation of XCH_4 seasonal cycle. These results also suggest the possibility that GOSAT and ACTM XCH_4 data can be used for correcting a priori emission scenarios by inverse modelling.

In contrast to the XCH_4 seasonal cycle over EIGP, a notable difference is observed in the emission and XCH_4 seasonal cycle over the SP region (Fig. 2b). The XCH_4 seasonal cycle and emission seasonal cycle are found to be out of phase with each other and the differences in emission scenarios are not reflected in XCH_4 seasonal variations. Both emission scenarios show the distinct seasonal pattern; AGS shows annual high emissions from April to September, while CTL shows annual high during August-September (Figure 3b7). The total emissions over SP are much lower than that of EIGP (note the different y-axis scale for Figure

3b7) and hence the difference between the XCH_4 simulations from both emission scenarios is comparatively low. The XCH_4 shows almost identical seasonal cycles for both of the emission scenarios, a peak in October and prolonged low values during May to September. The seasonal X_pCH_4 cycle in the LT layer shows the seasonal pattern similar to the total XCH_4. Inconsistency between emission seasonality and XCH_4 coupled with low emissions strongly suggests that the XCH_4 can be controlled by transport and/or chemistry, but not emissions. Surface winds during May - September over SP are of the marine origin, which effectively flushes the air with low CH_4 (see Figure S4). Further, the distinct seasonal cycle of chemical loss is observed over the SP region compared to other study regions; the loss rate starts increasing from 6 ppb day^{-1} in January to 12 ppb day^{-1} in April, and continue to remain high until September (ref. Figure S5). These pieces of evidence clearly suggest that the combined effect of transport and chemistry causes the low XCH_4 values for the May-September period over the SP region. The peaks in the upper layers in October (Figure 3b1-b4) and transport from the polluted continental layer in the LT layer (ref. Figure S4) could together contribute to the seasonal XCH_4 peak over SP. Based on these findings, we conclude that the XCH_4 measurements do not impose a strong constraint on surface emissions for inverse modelling over the SP region, suggesting a need for in situ measurements.

Over the Arid India (AI) region, XCH_4 seasonal cycle is observed to be different from those of the EIGP and SI regions. The simulated XCH_4 (Figure 3c6) show extremely weak sensitivity to the surface emission differences between the AGS and CTL cases (Figure 3c7). Additionally, the X_pCH_4 in the LT layer (Figure 3c5), does not resemble with the phase of seasonality in surface emissions and simulated/observed XCH_4. The X_pCH_4 in the LT layer decreases from Jan to August and increases until December. On the other hand, a remarkable peak (~1896 ppb) is observed in XCH_4 during August followed by a decline afterward (Figure 3c6). This is an outstanding example of deceiving linkage between surface emissions and XCH_4 in terms of seasonal variation. An enhancement in the mixing ratios of X_pCH_4 is observed from May to August only in the MT2 and UT layers (Figure 3c2-c3) and from June to August in the UA layer (Figure 3c1). This analysis infers that MT2 and UT partial columns mostly contribute in the formation of XCH_4 seasonal cycle over the AI region.

Next, we quantify the contributions of different partial layers (X_pCH_4) in the formation of XCH_4 seasonal amplitude (Figure 4). As the phase of $XpCH_4$ seasonal cycle does not always match with that of XCH_4, we have fixed months of peak and trough in XCH_4 seasonal cycle for this analysis. First, we calculate the differences of the X_pCH_4 values at the time of the peak and the trough of the XCH_4 over each region, and then the differences at different partial layers are divided by seasonal amplitude of XCH_4 for calculating the contributions from respective layers into the seasonal amplitude of XCH_4.

Figure 4 reveals that ~40% of the seasonal enhancement in the observed XCH_4 can be attributed to the partial pressure layers below 600 hPa (LT and MT1) for EIGP region, which is directly influenced by the surface emissions. About 40% in seasonal enhancement comes from layers above 600 hPa. Over the SP region, about 60% of the seasonal XCH_4 amplitude is attributed to layers below 600 hPa and remaining 40% results from the upper layers. Although the activities in the lower atmosphere (below 600 hPa) govern most of the seasonal XCH_4 cycle over this region, there is no clear link with seasonal variations in emissions as this region is under greater influence of changes in monsoon meteorology. These regions are under the influence of emission signals from the Indian subcontinent during winter; while in the summer, clean marine air control CH_4 levels (see also Patra et al., 2009). In contrast to the two regions mentioned above, over the AI region, the LT and MT1 layers together contribute only about 12% to the formation of XCH_4 seasonal cycle amplitude, and the layers above 600 hPa contribute to the remaining 88%. These

findings lead us to conclude that instead of surface emissions, the high CH_4 in the upper tropospheric layers contribute significantly to the formation of seasonal peaks in XCH_4.

3.3 Source of high CH_4 in the upper troposphere

The reason of high mixing ratios in the upper troposphere, as discussed in the former section, can be explained by vertical transport of high CH_4 emission signal from the surface, because the vertical transport time scales in the tropical region is much shorter than chemical lifetime of CH_4 of the order of 1-2 years (Patra et al., 2009). Figure 5a1-a4 shows the latitude-pressure crosssections of the convective transport rate (in ppb day^{-1}) and vertical velocity (hPa s^{-1}) averaged over 83-93°E for different seasons of 2011 (the ACTM AGS case). The positive/negative values of convective transport rate and vertical velocity in Figure 5a1-a4 indicate the gain/loss of mass and downward/upward motions, respectively. Rapid updrafts of CH_4, as indicated by higher negative vertical velocity, by deep convection during the monsoon season are aided by the regional topography of the IGP region (north of 20°N and east of 79°E in the Indian region). These updrafts lift CH_4-rich air into the upper tropospheric region (Figure 5b3). The CH_4 concentrations at the surface level decreased rapidly at an average rate of ~10 ppb day^{-1} during the SW monsoon season, and accumulate in the upper troposphere at a similar rate over IGP region (Figure 5a3). During the winter, spring and autumn season surface CH_4 decreased at an average rate of 2 ppb day^{-1}, 8 ppb day^{-1} and 7 ppb day^{-1}, respectively. CH_4 levels accumulate in the middle and upper troposphere at an average rate of 6 ppb day^{-1} during the spring and autumn season while during winter season no significant accumulation has been observed at this height over IGP region (Figure 5a1, a2, a4). Overall these transport processes repeat every year with a certain degree of interannual variations as can be seen for the years from 2011 to 2014. The interannual variations are likely to have been caused by the early/late onset and retreat of the SW monsoon as well as the weak/strong monsoon activity over the years.

The horizontal cross-sections of CH_4 at 200 hPa are shown with wind vectors in Figure 5c1-c4 for understanding the spatial extent of uplifted CH_4-rich air over the whole South Asian region. The uplifted CH_4-rich air mass is trapped in the upper troposphere (~200 hPa), when encountered by the anticyclonic winds during the SW monsoon season. This leads to a widespread CH_4 enhancement covering the large part of South Asia, and the CH_4-rich air leaked predominantly along the southern side of the sub-tropical westerly jet over to the East Asia (Figure 5c3; see also Umezawa et al., 2012). As a result of this, the high CH_4 air masses at upper troposphere are not limited to the regions of intense surface emissions as discussed earlier. After the SW monsoon season, the strong westerly jet breaks the upper tropospheric anticyclone and the CH_4 -rich air mass shifts over southern India during the autumn season (Figure 5c4). In this way, the convective updraft of high-CH_4 air mass, followed by horizontal spreading of the air mass over the larger area by anticyclonic circulation, controls the redistribution of CH_4 in the upper troposphere over the northern part of India during SW monsoon season, and over southern peninsula during the early autumn season.

4. Conclusions

The seasonal variations in dry-air mole fractions of methane (XCH_4) measured by GHGs Observation SATellite (GOSAT) are analyzed over India and the surrounding seas using the JAMSTEC's atmospheric chemistry-transport model (ACTM). The region of interest (Indian landmass) is divided into 8 sub-regions, namely, Northeast India (NEI), Eastern India (EI), Eastern IGP (EIGP), Western IGP (WIGP), Central India (CI), Arid India (AI), Western India (WI), Southern Peninsula (SP), and two

surrounding oceanic regions, the Arabian Sea (AS) and Bay of Bengal (BOB). The ACTM simulations are conducted using a couple of surface fluxes optimized by the inverse analysis as described in Patra et al. (2016). We have shown that the distinct spatial and temporal variations of XCH_4 observed by GOSAT are not only governed by the heterogeneity in surface emissions but also due to complex atmospheric transport mechanisms caused by the seasonally varying Asian monsoon. The seasonal XCH_4 patterns often show a fair correlation between emissions and XCH_4 over the regions residing in the northern half of India (north of 15^{o}N: NEI, EI, EIGP, WIGP, CI, WI, AI), which would imply XCH_4 levels are closely associated with the distribution of emissions on the Earth's surface. However, detailed analysis of transport and emission using ACTM over these regions (except for the AI) reveal that about 40% of seasonal enhancement in the observed XCH_4 can be attributed to the lower tropospheric layer (below 600 hPa). The lower tropospheric layer are either affected by the surface emissions, e.g., in the northern India regions or seasonal changes in horizontal winds due to monsoon for the SP region. Up to 40% of the seasonal CH_4 enhancement is found to come from the uplifted air mass in to the 600-200 hPa height layer over northern regions in India. In contrast, over semi-arid AI region, as much as ~88% contributions to the XCH_4 seasonal cycle amplitude came from the height above 600 hPa, and only ~12% are contributed by the atmosphere below 600 hPa. The primary cause of the higher contributions from above 600 hPa over the northern Indian region is the characteristic of air mass transport mechanisms in the Asian monsoon region. The persistent deep convection during the southwest monsoon season (June-August) causes strong updrafts of CH_4-rich air mass from the surface to upper tropospheric heights (~200 hPa), which is then confined by anticyclonic winds at this height. The anticyclonic confinement of surface emission over a wider South Asia region leads to strong contribution of the upper troposphere in formation of the XCH_4 peak over most regions in northern India, including the semi-arid regions with extremely low CH_4 emissions. In contrast to these regions, over the SP region, the major contributions (about 60%) to XCH_4 seasonal amplitude come from the lower atmosphere (~1000-600 hPa). Both transport and chemistry dominate in the lower troposphere over SP region and thus the formation of XCH_4 seasonal cycle is not consistent with the seasonal cycle of local emissions. As the upper level anticyclone does not cover the southern Indian region during the active phase of southwest monsoon, no enhancement in XCH_4 is observed over the southern peninsular region.

This study shows that ACTM simulations are well capturing the GOSAT observed seasonal and spatial XCH_4 variability and points to a comprehensive understanding of emissions, chemistry, and transport of CH_4 over one of the strongest global monsoonal regions. This provides extremely important for perceptive insights into the source-receptor relationships. Our results provide strong support for performing inverse modelling of CH_4 surface emissions in the future using XCH_4 observations and ACTM forward simulation.

Acknowledgements

The Environment Research and Technology Development Fund (A2-1502) of the Ministry of the Environment, Japan, supported this research. The data used for preparing the figures, and table could be available on request. The corresponding author may be contacted for the same.

References

Baker, A. K., Schuck, T. J., Brenninkmeijer, C. A. M., Rauthe-Schöch, A., Slemr, F., van Velthoven, P. F. J., and Lelieveld, J.: Estimating the contribution of monsoon-related biogenic production to methane emissions from South Asia using CARIBIC observations, Geophys. Res. Lett., 39, L10813, doi:10.1029/2012GL051756, 2012.

Crutzen. P.J., Aselmann, I., and Seiler, W.: Methane production by domestic animals, wild ruminants other herbivorous fauna and humans. Tellus 38B, 271-284, doi:10.1111/j.1600-0889.1986.tb00193.x, 1986.

Cao, M., Gregson, K., and Marshall, S.: Global methane emission from wetlands and its sensitivity to climate change. Atmos. Environ. 32 (19), 3293-3299, doi:10.1016/S1352-2310 (98) 00105-8, 1998.

Chandra, N., Venkataramani, S., Lal, S., Sheel, V. & Pozzer, A.: Effects of convection and long-range transport on the distribution of carbon monoxide in the troposphere over India. Atmospheric Pollution Research 7, 775 – 785, doi:10.1016/j.apr.2016.03.005, 2016.

Dlugokencky, E. J., Nisbet, E. G., Fisher, R., and Lowry, D.: Global atmospheric methane: Budget, changes, and dangers, Philos. Trans. R. Soc. London, Ser. A., 369, 2058–2072, 2011.

EDGAR42FT, 2013: Global emissions EDGAR v4.2FT2010 (October 2013). [Available at http://edgar.jrc.ec.europa.eu/overview.php?v=42FT2010.].

Fung, I., John, J., Lerner, J., Matthews, E., Prather, M., Steele, L. P., and Fraser, P. J.: Three-dimensional model synthesis of the global methane cycle, J. Geophys. Res., 96, 13033–13065, doi:10.1029/91JD01247, 1991

Frankenberg, C., P. Bergamaschi, A. Butz, S. Houweling, J. F. Meirink, J. Notholt, A. K. Petersen, H. Schrijver, T. Warneke, and I. Aben (2008), Tropical methane emissions: A revised view from SCIAMACHY onboard ENVISAT, *Geophys. Res. Lett.*, *35*(15), doi:10.1029/2008gl034300.

Frankenberg, C., I. Aben, P. Bergamaschi, E. J. Dlugokencky, R. van Hees, S. Houweling, P. van der Meer, R. Snel, and P. Tol (2011), Global column-averaged methane mixing ratios from 2003 to 2009 as derived from SCIAMACHY: Trends and variability, *J. Geophys. Res.*, *116*(D4), doi:10.1029/2010jd014849.

Gillett N. P. , and H. D. Matthews (2010), "Accounting For Carbon Cycle Feedbacks in a Comparison of the Global Warming Effects of Greenhouse Gases," Environ. Res. Lett. **5**, 034011 (2010).

Hayashida, S., Ono, A., Yoshizaki, S., Frankenberg, C., Takeuchi, W., Yan, X.: Methane concentrations over Monsoon Asia as observed by SCIAMACHY: Signals of methane emission from rice cultivation. Remote Sensing of Environment 139, 246–256, doi: 10.1016/j.rse.2013.08.008, 2013.

Kuze, A., Suto, H., Nakajima, M., and Hamazaki, T.: Thermal and near infrared sensor for carbon observation Fourier transform spectrometer on the Greenhouse Gases Observing Satellite for greenhouse gases monitoring. Appl. Opt. 48, 6716–6733, doi: 10.1364/AO.48.006716, 2009.

Kar, J., Deeter, M. N., Fishman, J., Liu, Z., Omar, A., Creilson, J. K., Trepte, C. R., Vaughan, M. A., and Winker, D. M.: Wintertime pollution over the Eastern Indo-Gangetic Plains as observed from MOPITT, CALIPSO and tropospheric ozone residual data, Atmos. Chem. Phys., 10, 12273-12283, doi:10.5194/acp-10-12273-2010, 2010.

Kavitha, M. and Nair, P. R.: Region-dependent seasonal pattern of methane over Indian region as observed by SCIAMACHY. Atmospheric Environment 131, 316–325, doi:10.1016/j.atmosenv.2016.02.008, 2016.

Lal, S., Venkataramani, S., Chandra, N., Cooper, O. R., Brioude, J., and Naja, M.: Transport effects on the vertical distribution of tropospheric ozone over western India, J. Geophys. Res. Atmos., 119, 10,012–10,026, doi:10.1002/ 2014JD021854, 2014.

Matthews, E., and Fung, I.: Methane emissions from natural wetlands: Global distribution, area and environmental characteristics of sources. Global Biogeochem. Cycles 1, 61-86, 1987.

Minami, K., and Neue, H. U.: Rice paddies as a methane source. Clim. Change Lett. 27, 13-26, doi:10.1007/BF01098470, 1994.

Morino, I., Uchino, O., Inoue, M., Yoshida, Y., Yokota, T., Wennberg, P. O., Toon, G. C., Wunch, D., Roehl, C. M., Notholt, J., Warneke, T., Messerschmidt, J., Griffith, D. W. T., Deutscher, N. M., Sherlock, V., Connor, B., Robinson, J., Sussmann, R.,

and Rettinger, M.: Preliminary validation of column-average volume mixing ratios of carbon dioxide and methane retrieved from GOSAT short-wavelength infrared spectra. Atmos. Meas. Tech., 4, 1061−1076, doi:10.5194/amt-4-1061-2011, 2011.

Myhre, G., Shindell, D., Bréon, F.-M., Collins, W. Fuglestvedt, J., Huang, J., Koch, D. Lamarque, J.-F., Lee, D., Mendoza, B., Nakajima, T., Robock, A., Stephens, G. Takemura, T., and Zhang, H.: Anthropogenic and natural radiative forcing, in: Climate Change 2013: The Physical Science Basis, Fifth Assessment Report of the Intergovernmental Panel on Climate Change, edited by: Stocker, T. F. et al., Cambridge University Press, Cambridge, UK, New York, NY, USA, 659–740, 2013.

Olivier, J. G. J., Aardenne, J.A.V., Dentener, F., Ganzeveld, L. N., Peters, J.A.H.W.:Recent trends in global greenhouse gas emissions: Regional trends and spatial distribution of key sources, in: Non-CO_2 Greenhouse Gases (NCGG-4), edited by: van Amstel, A., 325–330, Millpress, Rotterdam, Netherlands, 2005.

Onogi, K., Tsutsui, J., Koide, H., Sakamoto, M., Kobayashi, S., Hatsushika, H. Matsumoto, T., Yamazaki, N., Kamahori, H., Takahashi, K., Kadokura, S., Wada, K., Kato, K., Oyama, R., Ose, T., Mannoji, N., and Taira, R.: The JRA-25 reanalysis, J. Meteorol. Soc. Jpn., 85, 369–432, 2007.

Park, M., Randel, W. J., Kinnison, D. E., Garcia, R. R., and Choi, W.: Seasonal variation of methane, water vapor, and nitrogen oxides near the tropopause: Satellite observations and model simulations. Journal of Geophysical Research: Atmospheres 109, doi: 10.1029/2003JD003706. D03302, 2004.

Patra, P. K., Takigawa, M., Ishijima, K., Choi, B. C., Cunnold, D., Dlugokencky, E. J., Fraser, P., A. J., Gomez-Pelaez, Goo, T. Y., Kim, J. S., Krummel, P., Langenfelds, R., Meinhardt, F., Mukai, H., O'Doherty, S., Prinn, R. G., Simmonds, P., Steele, P., Tohjima, Y., Tsuboi, K., Uhse, K., Weiss, R., Worthy, D., and Nakazawa, T.: Growth rate, seasonal, synoptic, diurnal variations and budget of methane in lower atmosphere, J. Meteorol. Soc. Jpn., 87(4), 635-663, doi: 10.2151/jmsj.87.635, 2009.

Patra, P. K., Houweling, S., Krol, M., Bousquet, P., Belikov, D., Bergmann, D., Bian, H., Cameron-Smith, P., Chipperfield, M. P., Corbin, K., Fortems-Cheiney, A., Fraser, A., Gloor, E., Hess, P., Ito, A., Kawa, S. R., Law, R. M., Loh, Z., Maksyutov, S., Meng, L., Palmer, P. I., Prinn, R. G., Rigby, M., Saito, R., and Wilson, C.: TransCom model simulations of CH_4 and related species: Linking transport, surface flux and chemical loss with CH4 variability in the troposphere and lower stratosphere, Atmos. Chem. Phys., 11, 12,813–12,837, doi:10.5194/acp-11-12813-2011, 2011a.

Patra, P. K., Niwa, Y., Schuck, T. J., Brenninkmeijer, C. A. M., Machida, T., Matsueda, H., and Sawa, Y.: Carbon balance of South Asia constrained by passenger aircraft CO2 measurements, Atmos. Chem. Phys., 11, 4163-4175, doi:10.5194/acp-11-4163-2011, 2011b.

Patra, P. K., Canadell, J. G., Houghton, R. A., Piao, S. L., Oh, N.-H., Ciais, P., Manjunath, K. R., Chhabra, A., Wang, T., Bhattacharya, T., Bousquet, P., Hartman, J., Ito, A., Mayorga, E., Niwa, Y., Raymond, P. A., Sarma, V. V. S. S., and Lasco, R.: The carbon budget of South Asia, Biogeosciences, 10, 513-527, doi:10.5194/bg-10-513-2013, 2013.

Patra, P. K., Krol, M. C., Montzka, S. A., Arnold, T., Atlas, E. L., Lintner, B. R., Stephens, B. B., Xiang, B., Elkins, J. W., Fraser, P. J., Ghosh, A., Hintsa, E. J., Hurst, D. F., Ishijima, K., Krummel, P. B., Miller, B. R., Miyazaki, K., Moore, F. L., Mühle, J., O'Doherty, S., Prinn, R. G., Steele, L. P., Takigawa, M., Wang, H. J., Weiss, R. F., Wofsy, S. C., and Young, D.: Observational evidence for interhemispheric hydroxyl parity, Nature, 513, 219–223, 2014.

Patra, P. K., Saeki, T., Dlugokencky, E. J., Ishijima, K., Umezawa, 5 T., Ito, A., Aoki, S., Morimoto, S., Kort, E. A., Crotwell, A., Kumar, R., and Nakazawa, T.: Regional methane emission estimation based on observed atmospheric concentrations (2002–2012), J. Meteorol. Soc. Jpn., 94(1), 91–113, doi:10.2151/jmsj.2016-006, 2016.

Rao, Y. P.: Southwest monsoon: Synoptic Meteorology, Meteor. Monogr., No. 1/1976, India Meteorological Department, 367 pp, 1976.

Randel, W. J. and Park, M.: Deep convective influence on the Asian summer monsoon anticyclone and associated tracer variability observed with Atmospheric Infrared Sounder (AIRS). J. Geophys. Res. 111, doi: 10.1029/2005JD006490, 2006.

Sugimoto, A., Inoue, T., Kirtibutr, N. and Abe, T.: Methane oxidation by termite mounds estimated by the carbon isotopic composition of methane. Glob. Biogeochem. Cycles 12 (4), 595-605, doi:10.1029/98GB02266, 1998.

Shindell, D. T., Faluvegi, G., Koch, D. M., Schmidt, G. A., Unger, N., Bauer, S. E.: Improved attribution of climate forcing to emissions, Science, 326, 716-718, doi: 10.1126/science.1174760, 2009.

Schuck, T. J., Ishijima, K., Patra, P. K., Baker, A. K., Machida, T., Matsueda, H., Sawa, Y., Umezawa, T., Brenninkmeijer, C. A. M., and Lelieveld, J.: Distribution of methane in the tropical upper troposphere measured by CARIBIC and CONTRAIL aircraft, J. Geophys. Res.,117, D19304, doi:10.1029/2012JD018199, 2012.

Spivakovsky, C. M., Logan, J. A., Montzka, S. A., Balkanski, Y. J., Foreman-Fowler, M., Jones, D. B. A., Horowitz, L. W.,Fusco, A. C., Brenninkmeijer, C. A. M., Prather, M. J., Wofsy, S. C., and McElroy, M. B.: Three-dimensional climatological distribution of tropospheric OH: update and evaluation, J. Geophys. Res., 105, 8931–8980, doi:10.1029/1999JD901006, 2000.

Umezawa, T., Machida, T., Ishijima, K., Matsueda, H., Sawa, Y., Patra, P. K., Aoki, S., and Nakazawa, T. Carbon and hydrogen isotopic ratios of atmospheric methane in the upper troposphere over the Western Pacific, Atmos. Chem. Phys., 12, 8095-8113, 2012.

Wunch, D., G. C. Toon, J.-F. L. Blavier, R. A. Washenfelder, J. Notholt, B. J. Connor, D. W. T. Griffith, V. Sherlock, and P. O. Wennberg, The total carbon column observing network, Phil. Trans. Royal Society - Series A, 369, 2087-2112, doi:10.1098/rsta.2010.0240, 2011.

Xiong, X., Houweling, S., Wei, J., Maddy, E., Sun, F., and Barnet, C.: Methane plume over south Asia during the monsoon season: satellite observation and model simulation, Atmos. Chem. Phys., 9, 783-794, doi:10.5194/acp-9-783-2009, 2009.

Yoshida, Y., Y. Ota, N. Eguchi, N. Kikuchi, K. Nobuta, H. Tran, I. Morino, and T. Yokota (2011), Retrieval algorithm for CO_2 and CH_4 column abundances from short-wavelength infrared spectral observations by the Greenhouse gases observing satellite, *Atmospheric Measurement Techniques*, *4*(4), 717-734, doi:10.5194/amt-4-717-2011.

Yoshida, Y., Kikuchi, N., Morino, I., Uchino, O., Oshchepkov, S., Bril, A., Saeki, T., Schutgens, N., Toon, G. C., Wunch, D., Roehl, C. M., Wennberg, P. O., Griffith, D. W. T., Deutscher, N. M.,Warneke, T., Notholt, J., Robinson, J., Sherlock, V., Connor, B., Rettinger, M., Sussmann, R., Ahonen, P., Heikkinen, P., Kyrö, E., Mendonca, J., Strong, K., Hase, F., Dohe, S., and Yokota, T.: Improvement of the retrieval algorithm for GOSAT SWIRXCO_2 and XCH_4 and their validation using TCCON data, Atmos. Meas. Tech., 6, 1533–1547, doi:10.5194/amt-6-1533-2013, 2013.

Yan, X., Akiyama, H., Yagi, K., and Akimoto, H.: Global estimations of the inventory and mitigation potential of methane emissions from rice cultivation conducted using the 2006 Intergovernmental Panel on Climate Change Guidelines, Global Biogeochem. Cycles, 23, GB2002, doi:10.1029/2008GB003299, 2009.

Figures and Table.

Table S1: Correlation coefficients (r) between observed and model simulated seasonal cycles of XCH_4. Model simulations are obtained from ACTM using two different emission scenarios, AGS and CTL.

Site/ Tracer	ACTM_AGS	ACTM_CTL
Arid India	0.77	0.88
WIGP region	0.86	0.90
EIGP region	0.69	0.88
Northeast India	0.55	0.55
Western India	0.87	0.95
Central India	0.89	0.97
East India	0.78	0.86
Southern Peninsula	0.92	0.91
Arabian Sea	0.86	0.87
Bay of Bengal	0.84	0.86

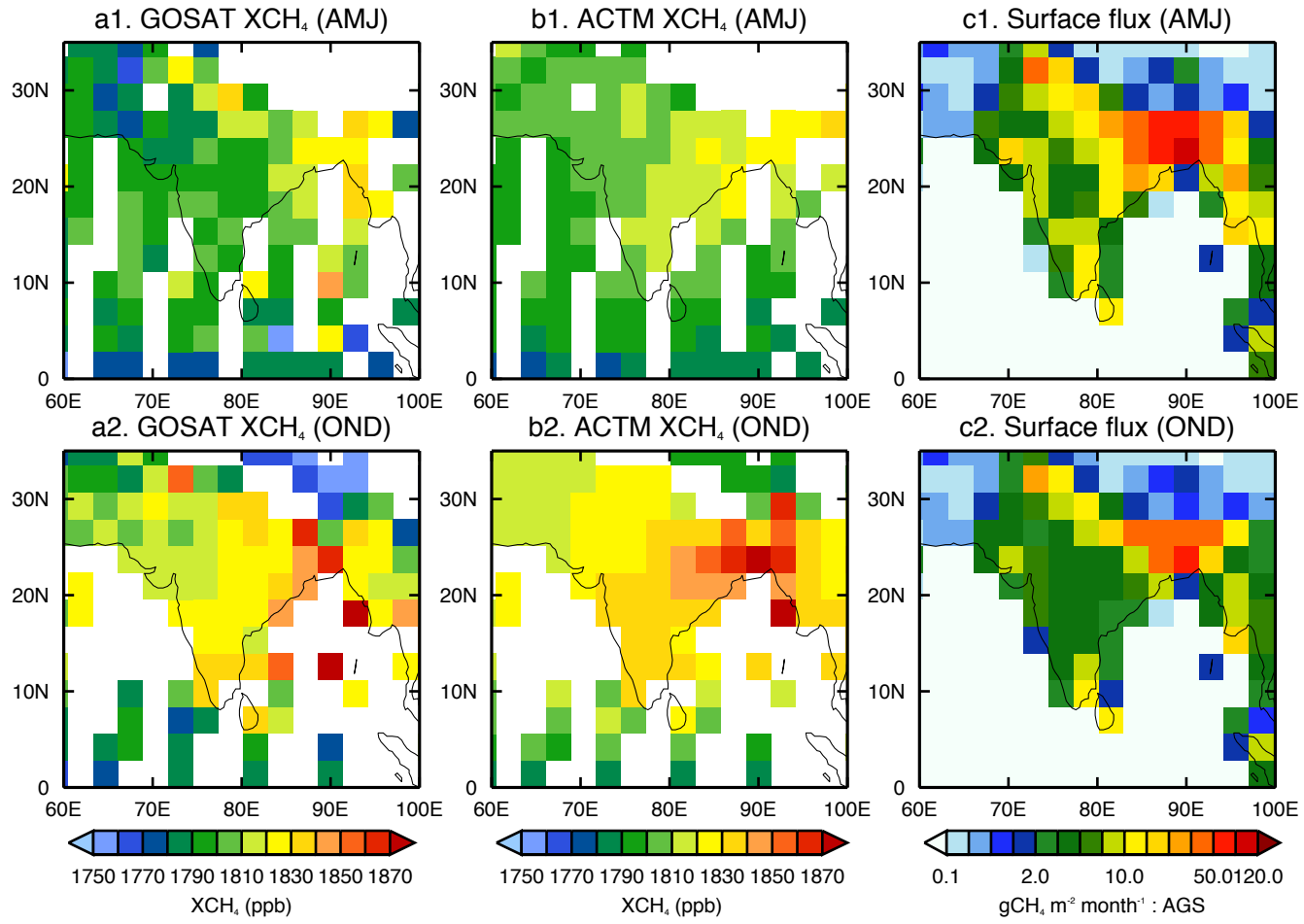

Figure 1: Average seasonal distributions (from 2011 to 2014) of XCH_4 obtained from GOSAT observations (a1-a2), ACTM simulations (b1-b2) and CH_4 emission consisting of all the natural and anthropogenic emissions (c1-c2: ACTM_AGS case) over the Indian region. Optimized emissions are shown from a global inversion of surface CH_4 concentrations (Patra et al., 2016) and multiplied by a constant factor of 12 for a clear visualization. The ACTM is first sampled at the location and time of GOSAT observations and then seasonally averaged. The white spaces in panels (a1-b2) are due to the missing data caused by satellite retrieval limitations from cloud cover.

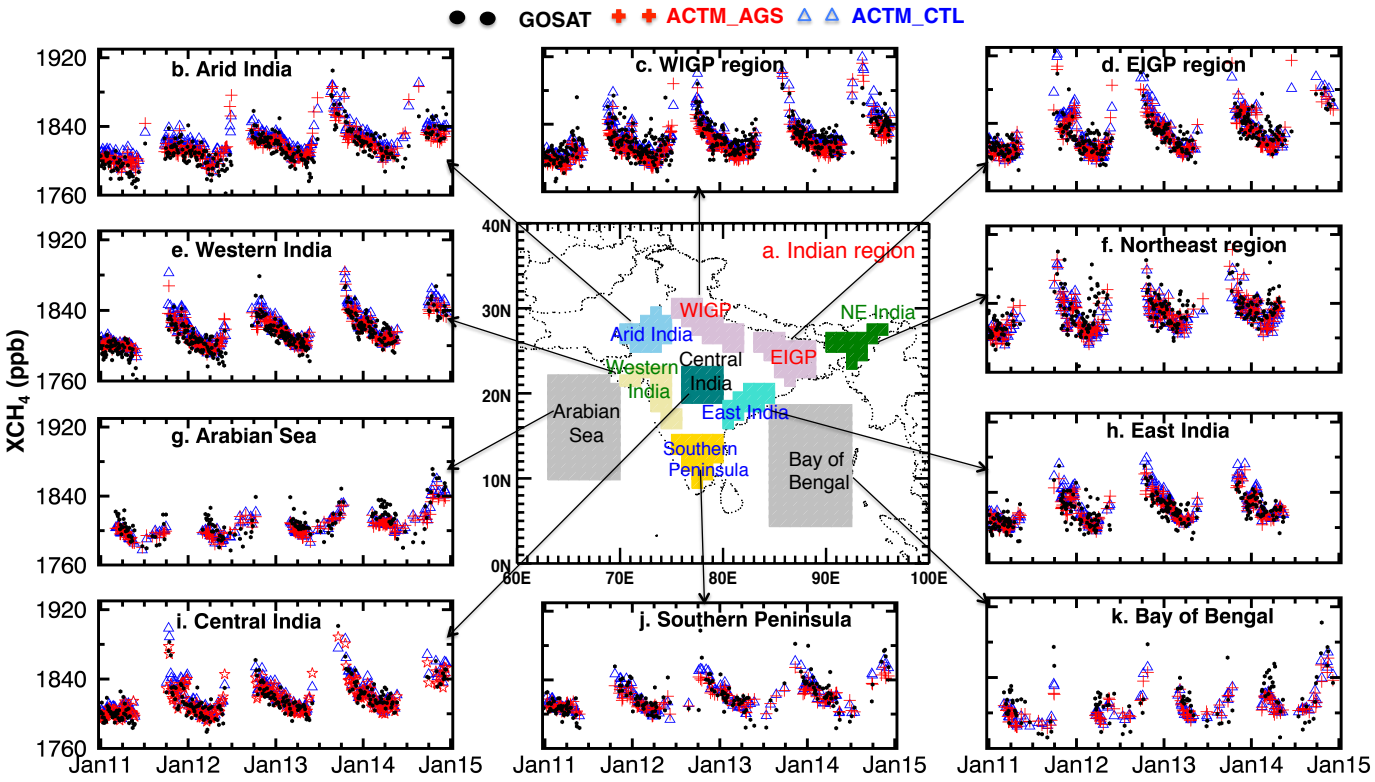

Figure 2: (a) The map of the regional divisions (shaded) for the time series analysis. (b-l) Time series of XCH_4 over the selected regions (shown in map) as obtained from GOSAT and simulated by ACTM for two different emission scenarios, namely, ACTM_AGS and ACTM_CTL. The gaps are due to the missing observational data.

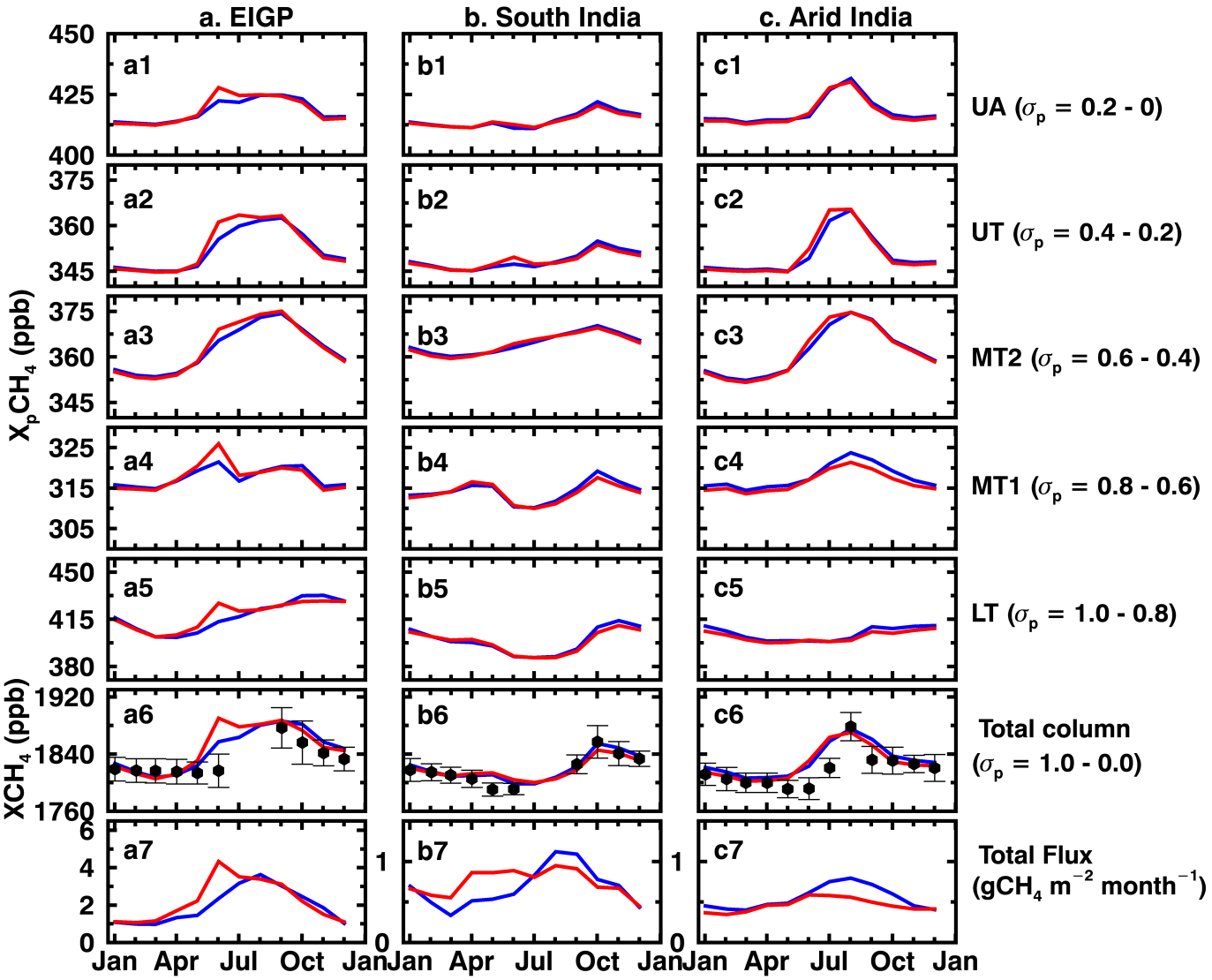

Figure 3: The bottom panels show the monthly mean climatology of the total optimized CH_4 emissions (panels a7, b7, c7); estimated after performing the global inverse analysis (Patra et al., 2016). The second bottom panels show XCH_4 obtained from the GOSAT observations (black circles in panels a6, b6, c6) and ACTM simulations (panels a6, b6, c6) over the Eastern IGP (a: first column), Southern Peninsula (b: second column) and Arid India region (c: third column). Monthly climatology is based on the monthly mean values for the period of 2011-2014 for all the values. The error bars in the GOSAT monthly mean values depict the 1-sigma standard deviations for the corresponding months (a6, b6, c6). The 1-sigma values are not plotted for the model simulations to maintain figure clarity. Simulations are based on two different emission scenarios namely ACTM_CTL (blue lines) and ACTM_AGS (red lines) based on the different combinations of emissions. The upper five panels show the monthly climatology of partial columnar methane (denoted by X_pCH_4) calculated at five different partial sigma-pressure layers; 1.0-0.8 (a5, b5, c5), 0.8-0.6 (a4, b4, c4), 0.6-0.4 (a3, b3, c3), 0.4-0.2 (a2, b2, c2) and 0.2-0.0 (a1, b1, c1). Please note that the y scales in the emission plots over southern peninsula and Arid India (b7 and c7) are different from over the EIGP region (a7).

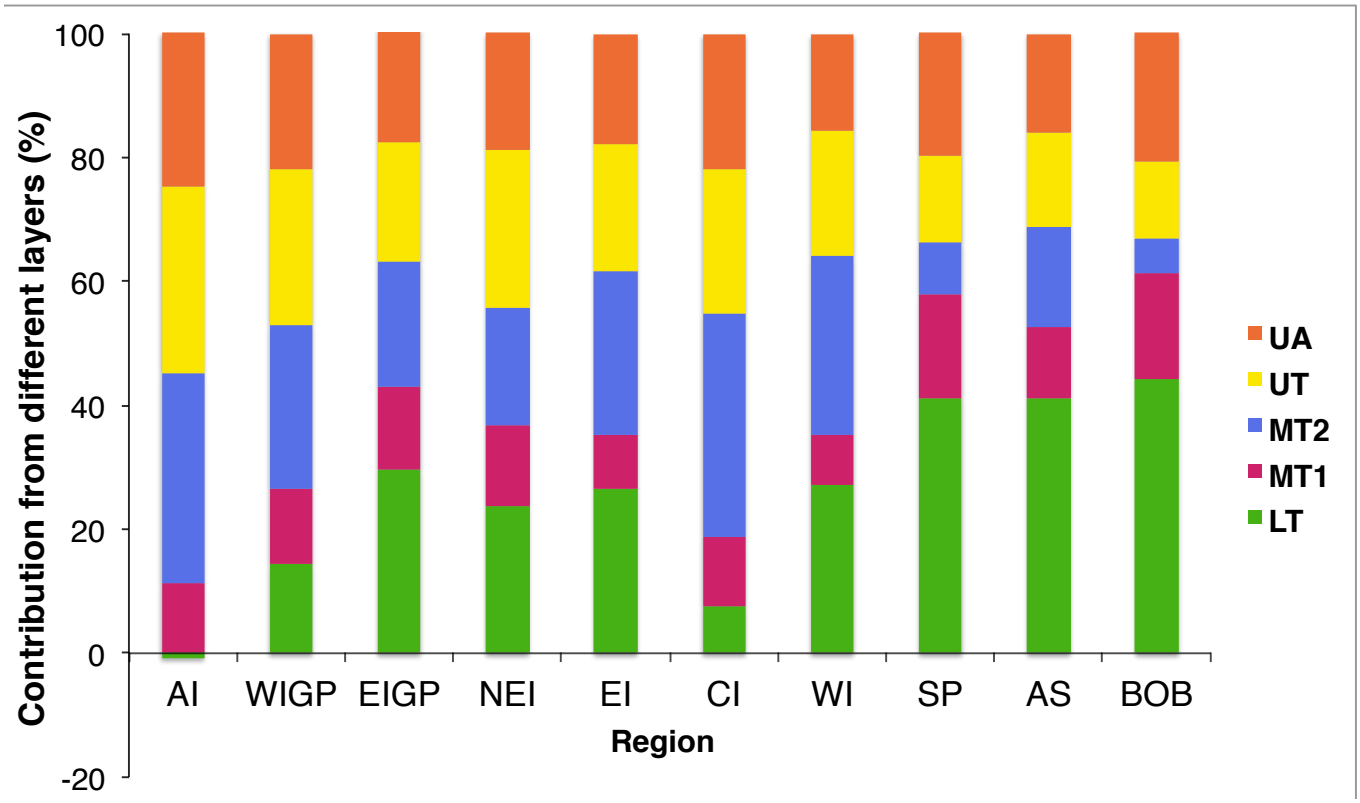

Figure 4: Contributions of partial columns in the seasonal amplitude of XCH_4 over selected regions for AGS case. Differences in the X_pCH_4, calculated at the same time as the maxima and minima of the seasonal XCH_4 cycle, are used to calculate the percentage contributions of respective partial columns in the seasonal amplitude of XCH_4.

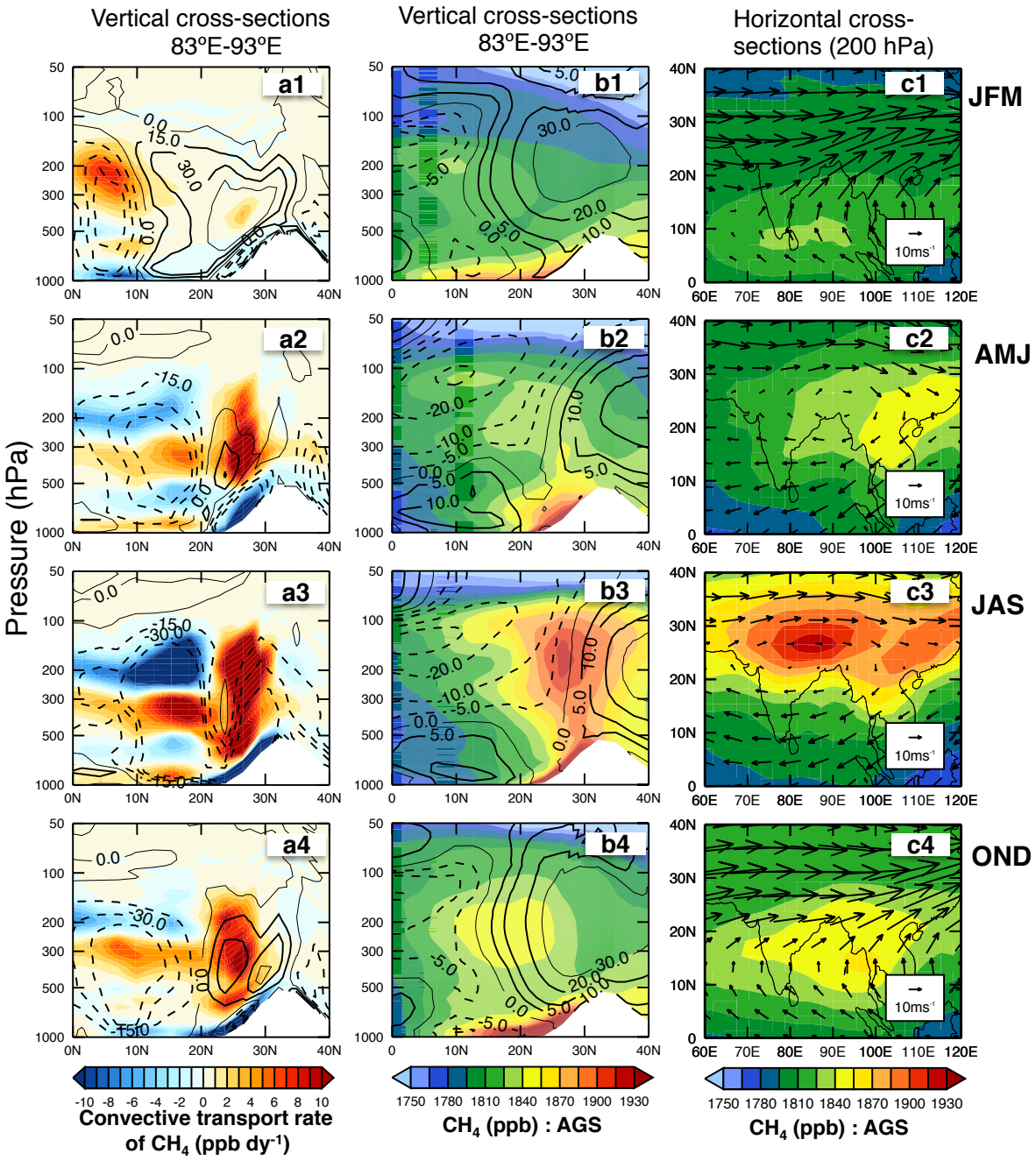

Figure 5: Vertical structure of seasonally averaged CH_4 transport rate due to the convection (a1-a4, in ppb day^{-1}) and CH_4 mixing ratios (b1-b4 from AGS scenarios) averaged over 83-93°E for the year 2011. Positive and negative transport rate values represent the accumulation and dissipation of mass, respectively. The contour lines in the first (a1-a4) and second (b1-b4) columns depict the average omega velocity (in hPa s^{-1}) and u wind component, respectively for the same period. The solid contour lines show the positive values and dotted lines show negative values. Positive and negative values of the omega velocity represent downward and upward motions, respectively. The zero value of u wind indicates that the wind is either purely southerly or northerly. White spaces in zonal-mean plots (a1- b4) show the missing data due to orography. The rightmost column (c1-c4) depicts the maps of averaged CH_4 and wind vectors (in m s^{-1}; arrow) during all the four seasons in 2011 at 200 hPa height.